DESY 94-030
March 1994
ISSN 0418-9833

Inclusive Charged Particle Cross Sections in Photoproduction at HERA

H1 Collaboration

Abstract:

Cross sections are presented for the inclusive production of charged particles measured in electron-proton collisions at low Q^2 with the H1 detector at HERA. The transverse momentum distribution extends up to 8 GeV/c. Its shape is found to be harder than that observed in $\bar{p}p$ collisions at comparable centre-of-mass energies $\sqrt{s_{\gamma p}} \approx \sqrt{s_{\bar{p}p}} \approx 200$ GeV, and also harder than in γp collisions at lower energies $\sqrt{s_{\gamma p}} \approx 18$ GeV. Results from quantum chromodynamics (QCD) calculations agree with the measured transverse momentum and pseudorapidity cross sections.

submitted to Physics Letters B

H1 Collaboration

I. Abt[7], T. Ahmed[3], V. Andreev[24], S. Aid[13], B. Andrieu[27], R.-D. Appuhn[11], M. Arpagaus[34], A. Babaev[25], H. Bärwolff[33], J. Bán[17], P. Baranov[24], E. Barrelet[28], W. Bartel[11], U. Bassler[28], H.P. Beck[35], H.-J. Behrend[11], A. Belousov[24], Ch. Berger[1], H. Bergstein[1], G. Bernardi[28], R. Bernet[34], G. Bertrand-Coremans[4], M. Besançon[9], P. Biddulph[22], E. Binder[11], J.C. Bizot[26], V. Blobel[13], K. Borras[8], P.C. Bosetti[2], V. Boudry[27], C. Bourdarios[26], A. Braemer[14], F. Brasse[11], U. Braun[2], W. Braunschweig[1], V. Brisson[26], D. Bruncko[17], L. Büngener[13], J. Bürger[11], F.W. Büsser[13], A. Buniatian[11,37], S. Burke[19], G. Buschhorn[25], A.J. Campbell[1], T. Carli[25], F. Charles[28], J. Chyla[29], D. Clarke[5], A.B. Clegg[18], M. Colombo[8], J.A. Coughlan[5], A. Courau[26], Ch. Coutures[9], G. Cozzika[9], L. Criegee[11], J. Cvach[29], S. Dagoret[28], J.B. Dainton[19], M. Danilov[23], A.W.E. Dann[22], W.D. Dau[16], M. David[9], E. Deffur[11], B. Delcourt[26], L. Del Buono[28], M. Devel[26], A. De Roeck[11], P. Di Nezza[31], P. Dingus[27], C. Dollfus[35], J.D. Dowell[3], H.B. Dreis[2], A. Drescher[8], J. Duboc[28], D. Düllmann[13], O. Dünger[13], H. Duhm[12], R. Ebbinghaus[8], M. Eberle[12], J. Ebert[32], T.R. Ebert[19], G. Eckerlin[11], V. Efremenko[23], S. Egli[35], H. Ehrlichmann[33], S. Eichenberger[35], R. Eichler[34], F. Eisele[14], E. Eisenhandler[20], N.N. Ellis[3], R.J. Ellison[22], E. Elsen[11], M. Erdmann[14], E. Evrard[4], L. Favart[4], A. Fedotov[23], D. Feeken[13], R. Felst[11], J. Feltesse[9], I.F. Fensome[3], J. Ferencei[11], F. Ferrarotto[31], K. Flamm[11], W. Flauger[11,†], M. Fleischer[11], M. Flieser[25], G. Flügge[2], A. Fomenko[24], B. Fominykh[23], M. Forbush[7], J. Formánek[30], J.M. Foster[22], G. Franke[11], E. Fretwurst[12], P. Fuhrmann[1], E. Gabathuler[19], K. Gamerdinger[25], J. Garvey[3], J. Gayler[11], M. Gebauer[8], A. Gellrich[13], M. Gennis[11], H. Genzel[1], R. Gerhards[11], L. Godfrey[7], U. Goerlach[11], L. Goerlich[6], N. Gogitidze[24], M. Goldberg[28], D. Goldner[8], A.M. Goodall[19], I. Gorelov[23], P. Goritchev[23], C. Grab[34], H. Grässler[2], R. Grässler[2], T. Greenshaw[19], H. Greif[25], G. Grindhammer[25], A. Gruber[25], C. Gruber[16], J. Haack[33], D. Haidt[11], L. Hajduk[6], O. Hamon[28], M. Hampel[1], E.M. Hanlon[18], M. Hapke[11], J. Harjes[11], R. Haydar[26], W.J. Haynes[5], J. Heatherington[20], V. Hedberg[21], G. Heinzelmann[13], R.C.W. Henderson[18], H. Henschel[33], R. Herma[1], I. Herynek[29], W. Hildesheim[11], P. Hill[5], C.D. Hilton[22], J. Hladký[29], K.C. Hoeger[22], M. Höppner[8], Ph. Huet[4], H. Hufnagel[14], N. Huot[28], M. Ibbotson[22], H. Itterbeck[1], M.-A. Jabiol[9], A. Jacholkowska[26], C. Jacobsson[21], M. Jaffre[26], T. Jansen[11], L. Jönsson[21], K. Johannsen[13], D.P. Johnson[4], L. Johnson[18], H. Jung[11], P.I.P. Kalmus[20], D. Kant[20], S. Kazarian[11], R. Kaschowitz[2], P. Kasselmann[12], U. Kathage[16], H.H.Kaufmann[33], I.R. Kenyon[3], S. Kermiche[26], C. Keuker[1], C. Kiesling[25], M. Klein[33], C. Kleinwort[13], G. Knies[11], W. Ko[7], T. Köhler[1], H. Kolanoski[8], F. Kole[7], S.D. Kolya[22], V. Korbel[11], M. Korn[8], P. Kostka[33], S.K. Kotelnikov[24], M.W. Krasny[6,28], H. Krehbiel[11], D. Krücker[2], U. Krüger[11], J.P. Kubenka[25], H. Küster[2], M. Kuhlen[25], T. Kurča[17], J. Kurzhöfer[8], B. Kuznik[32], D. Lacour[28], F. Lamarche[27], R. Lander[7], M.P.J. Landon[20], W. Lange[33], R. Langkau[12], P. Lanius[25], J.F. Laporte[9], A. Lebedev[24], A. Leuschner[11], C. Leverenz[11], S. Levonian[11,24], D. Lewin[11], Ch. Ley[2], A. Lindner[8], G. Lindström[12], F. Linsel[11], J. Lipinski[13], P. Loch[11], H. Lohmander[21], G.C. Lopez[20], D. Lüers[25,†], D. Lüke[8,11], N. Magnussen[32], E. Malinovski[24], S. Mani[7], P. Marage[4], J. Marks[10], R. Marshall[22], J. Martens[32], R. Martin[19], H.-U. Martyn[1], J. Martyniak[6], S. Masson[2], A. Mavroidis[20], S.J. Maxfield[19], S.J. McMahon[19], A. Mehta[22], K. Meier[15], D. Mercer[22], T. Merz[11], C.A. Meyer[35], H. Meyer[32], J. Meyer[11], S. Mikocki[6,26], E. Monnier[28], F. Moreau[27], J. Moreels[4], J.V. Morris[5], K. Müller[35], P. Murín[17], S.A. Murray[22], V. Nagovizin[23], B. Naroska[13], Th. Naumann[33], P.R. Newman[3], D. Newton[18], D. Neyret[28], H.K. Nguyen[28], F. Niebergall[13], C. Niebuhr[11], R. Nisius[1], G. Nowak[6], G.W. Noyes[3], M. Nyberg[21], H. Oberlack[25], U. Obrock[8], J.E. Olsson[11], S. Orenstein[27], F. Ould-Saada[13], C. Pascaud[26], G.D. Patel[19], E. Peppel[11], S. Peters[25], H.T. Phillips[3], J.P. Phillips[22], Ch. Pichler[12], W. Pilgram[2], D. Pitzl[34], S. Prell[11], R. Prosi[11], G. Rädel[11], F. Raupach[1], K. Rauschnabel[8], P. Reimer[29], S. Reinshagen[11], P. Ribarics[25], V. Riech[12], J. Riedlberger[34], S. Riess[13], M. Rietz[2], S.M. Robertson[3], P. Robmann[35], R. Roosen[4], K. Rosenbauer[1] A. Rostovtsev[23], C. Royon[9], M. Rudowicz[25], M. Ruffer[12], S. Rusakov[24], K. Rybicki[6],

N. Sahlmann[2], E. Sanchez[25], D.P.C. Sankey[5], M. Savitsky[11], P. Schacht[25], P. Schleper[14], W. von Schlippe[20], C. Schmidt[11], D. Schmidt[32], W. Schmitz[2], A. Schöning[11], V. Schröder[11], E. Schuhmann[25], M. Schulz[11], B. Schwab[14], A. Schwind[33], W. Scobel[12], U. Seehausen[13], R. Sell[11], A. Semenov[23], V. Shekelyan[23], I. Sheviakov[24], H. Shooshtari[25], L.N. Shtarkov[24], G. Siegmon[16], U. Siewert[16], Y. Sirois[27], I.O. Skillicorn[10], P. Smirnov[24], J.R. Smith[7], Y. Soloviev[24], H. Spitzer[13], M. Steenbock[13], P. Steffen[11], R. Steinberg[2], B. Stella[31], K. Stephens[22], J. Stier[11], U. Stösslein[33], J. Strachota[29], U. Straumann[35], W. Struczinski[2], J.P. Sutton[3], R.E. Taylor[36,26], V. Tchernyshov[23], C. Thiebaux[27], G. Thompson[20], I. Tichomirov[23], P. Truöl[35], J. Turnau[6], J. Tutas[14], L. Urban[25], A. Usik[24], S. Valkar[30], A. Valkarova[30], C. Vallée[28], P. Van Esch[4], A. Vartapetian[11,37], Y. Vazdik[24], M. Vecko[29], P. Verrecchia[9], R. Vick[13], G. Villet[9], E. Vogel[1], K. Wacker[8], I.W. Walker[18], A. Walther[8], G. Weber[13], D. Wegener[8], A. Wegner[11], H. P.Wellisch[25], L.R. West[3], S. Willard[7], M. Winde[33], G.-G. Winter[11], Th. Wolff[34], L.A. Womersley[19], A.E. Wright[22], N. Wulff[11], T.P. Yiou[28], J. Žáček[30], C. Zeitnitz[12], H. Ziaeepour[26], M. Zimmer[11], W. Zimmermann[11] and F. Zomer[26]

[1] *I. Physikalisches Institut der RWTH, Aachen, Germany*[a]
[2] *III. Physikalisches Institut der RWTH, Aachen, Germany*[a]
[3] *School of Physics and Space Research, University of Birmingham, Birmingham, UK*[b]
[4] *Inter-University Institute for High Energies ULB-VUB, Brussels, Belgium*[c]
[5] *Rutherford Appleton Laboratory, Chilton, Didcot, UK*[b]
[6] *Institute for Nuclear Physics, Cracow, Poland*[d]
[7] *Physics Department and IIRPA, University of California, Davis, California, USA*[e]
[8] *Institut für Physik, Universität Dortmund, Dortmund, Germany*[a]
[9] *DAPNIA, Centre d'Etudes de Saclay, Gif-sur-Yvette, France*
[10] *Department of Physics and Astronomy, University of Glasgow, Glasgow, UK*[b]
[11] *DESY, Hamburg, Germany*[a]
[12] *I. Institut für Experimentalphysik, Universität Hamburg, Hamburg, Germany*[a]
[13] *II. Institut für Experimentalphysik, Universität Hamburg, Hamburg, Germany*[a]
[14] *Physikalisches Institut, Universität Heidelberg, Heidelberg, Germany*[a]
[15] *Institut für Hochenergiephysik, Universität Heidelberg, Heidelberg, Germany*[a]
[16] *Institut für Reine und Angewandte Kernphysik, Universität Kiel, Kiel, Germany*[a]
[17] *Institute of Experimental Physics, Slovak Academy of Sciences, Košice, Slovak Republik*
[18] *School of Physics and Materials, University of Lancaster, Lancaster, UK*[b]
[19] *Department of Physics, University of Liverpool, Liverpool, UK*[b]
[20] *Queen Mary and Westfield College, London, UK*[b]
[21] *Physics Department, University of Lund, Lund, Sweden*[f]
[22] *Physics Department, University of Manchester, Manchester, UK*[b]
[23] *Institute for Theoretical and Experimental Physics, Moscow, Russia*
[24] *Lebedev Physical Institute, Moscow, Russia*
[25] *Max-Planck-Institut für Physik, München, Germany*[a]
[26] *LAL, Université de Paris-Sud, IN2P3-CNRS, Orsay, France*
[27] *LPNHE, Ecole Polytechnique, IN2P3-CNRS, Palaiseau, France*
[28] *LPNHE, Universités Paris VI and VII, IN2P3-CNRS, Paris, France*
[29] *Institute of Physics, Czech Academy of Sciences, Praha, Czech Republik*
[30] *Nuclear Center, Charles University, Praha, Czech Republik*
[31] *INFN Roma and Dipartimento di Fisica, Universita "La Sapienza", Roma, Italy*
[32] *Fachbereich Physik, Bergische Universität Gesamthochschule Wuppertal, Wuppertal, Germany*[a]
[33] *DESY, Institut für Hochenergiephysik, Zeuthen, Germany*[a]
[34] *Institut für Teilchenphysik, ETH, Zürich, Switzerland*[g]
[35] *Physik-Institut der Universität Zürich, Zürich, Switzerland*[g]
[36] *Stanford Linear Accelerator Center, Stanford California, USA*

[37] *Visitor from Yerevan Phys.Inst., Armenia*

† *Deceased*

[a] *Supported by the Bundesministerium für Forschung und Technologie, FRG under contract numbers 6AC17P, 6AC47P, 6DO57I, 6HH17P, 6HH27I, 6HD17I, 6HD27I, 6KI17P, 6MP17I, and 6WT87P*

[b] *Supported by the UK Science and Engineering Research Council*

[c] *Supported by IISN-IIKW, NATO CRG-890478*

[d] *Supported by the Polish State Committee for Scientific Research, grant No. 204209101*

[e] *Supported in part by USDOE grant DE F603 91ER40674*

[f] *Supported by the Swedish Natural Science Research Council*

[g] *Supported by the Swiss National Science Foundation*

1 Introduction

The electron-proton collider HERA is an important research facility for the understanding of the photon. Quasi-real photons are produced in ep collisions by electrons which are scattered through small angles. In the photon-proton collisions centre-of-mass (CMS) energies up to 300 GeV can be reached. This is one order of magnitude larger than the CMS energies achieved so far in fixed target experiments. At this energy hard scattering processes can reveal the underlying dynamics of the constituents of hadrons [1].

The photon, gauge boson of the electromagnetic interactions, couples directly to charged matter, e.g to a quark of the proton. In addition vacuum fluctuations of an energetic photon into, for example, a vector meson enable the photon to interact strongly with a proton. These indirect photon-proton interactions are termed *resolved* photoproduction processes, in order to distinguish them from the *direct* processes mentioned first. The resolved photon component with its large strong interaction cross section has been shown to dominate the direct processes at HERA at moderate transverse momenta (p_T) [2, 3]. The existence of direct processes has been demonstrated in refs.[4, 5].

A part of the resolved photoproduction has been known for about 30 years and is phenomenologically described by the vector dominance model (VDM) [6, 7]. Here the photon is pictured to fluctuate into a vector meson with the same quantum numbers as the photon. In this case the photon-hadron interaction follows essentially the same phenomenology as a hadron-hadron collision.

However, the pointlike coupling of the photon to quarks leads to another component in resolved photoproduction where the photon splits into a $q\overline{q}$ pair, without forming a bound state. This additional part is referred to as the *anomalous* or *pointlike* component which has been demonstrated in two-photon processes (e.g.[8]).

At HERA the majority of photoproduction interactions consists of low transverse momentum peripheral collisions, similar to hadron-hadron interactions, *i.e.,* collisions where the hadronic final state kinematics is essentially described by longitudinal phase space. Hereafter, they will be termed *soft processes.* In addition, *hard processes*, *i.e.,* hard scattering in γp interactions, are expected from partonic collisions between quarks and gluons of the incident proton and the resolved photon, and from the direct production diagrams (boson gluon fusion and QCD Compton scattering). The contributions of these latter diagrams to the γp cross section can be calculated in perturbative QCD. For resolved collisions this picture leads to the introduction of a photon structure function describing probabilities of finding partons in the photon with a certain momentum fraction, x_γ, of the photon at a typical scale p_T^2 of the momentum transfer in a given process. Parametrizations of the photon structure function as used to analyse photoproduction at HERA are obtained by perturbative QCD evolutions of both the VDM and anomalous pieces (e.g. [9]). With a leading logarithmic behaviour like $\log(p_T^2/\Lambda_{QCD}^2)$ [10] the anomalous component of the photon is expected to dominate in resolved reactions with large momentum transfer.

With the first data taken at HERA this general picture of hard photon-proton scattering has been confirmed by studying single particle distributions [2] and jet topologies [3, 11]. In this letter we present the measurement of charged particle cross sections in photoproduction events, based on data collected in 1992 with the H1 detector. The measurements are compared with experimental results from a $\bar{p}p$-collider experiment (UA1 collaboration [12]) at $\sqrt{s_{\bar{p}p}} =$ 200 GeV, and from a fixed target experiment (WA69 collaboration [4]) at $\sqrt{s_{\gamma p}} = 18$ GeV. Since both the direct and anomalous components are absent in hadron-hadron interactions, we expect differences in the charged particle distributions between $hadron - proton$ and $\gamma - proton$ collisions.

In the region of transverse momenta (p_T) of charged particles above 1.5 GeV/c we compare the cross sections with two QCD calculations: the first is based on leading-order (LO) QCD plus a parton shower model, the second is a next-to-leading order (NLO) calculation.

2 Experimental Setup

The HERA ep storage ring was operated in 1992 with 9 colliding bunches of e^- and p, with energies of 26.7 GeV and 820 GeV , respectively. In addition, both electron and proton beams featured a *pilot bunch*, *i.e.,* a beam bunch with no corresponding collision partner bunch in the other beam with which to collide in the interaction region. This allows the beam related background to be measured.

A detailed description of the H1-detector has been given elsewhere [13]. Hence, only the components crucial for this particular analysis are described below.

The H1-luminosity system consists of an electron detector and a photon detector, located 33 m and 103 m from the interaction point in the electron beam direction (backward, *i.e.,* downstream w.r.t. electron beam), respectively. The luminosity is determined from the rate of Bethe-Heitler $ep \to ep\gamma$ events by detecting the scattered electron and the photon. Both detectors are TlCl/TlBr crystal Čerenkov calorimeters with an energy resolution of $10\%/\sqrt{E}$. The integrated luminosity used for this analysis was 19 nb^{-1} measured with an accuracy of 7%. In addition, the electron detector tags also photoproduction events by detecting electrons scattered at small angles.

Measurements of charged tracks are provided by two cylindrical drift chambers [14], mounted concentrically around the beamline inside a homogeneous magnetic field of 1.2 Tesla. Up to 56 space points are measured for a track yielding particle charge and momentum from the track curvature in the polar angular range of 20° and 160°. The resolution for the momentum measurement in the $x-y$ plane transverse to the beam direction (proton beam in $+z$ direction) is $\sigma(p_T)/p_T \approx 0.009 \cdot p_T\ (\mathrm{GeV}/c)^{-1} \oplus 0.015$. The resolution for the polar angle θ is 20 mrad.

A ray trigger is provided by two cylindrical multiwire proportional chambers (MWPC), which are positioned inside (CIP) and in between (COP) the two drift chambers. Each consists of two independent MWPCs with pads at the inner and outer radius [15]. Charged tracks originating from the interaction region produce a ray trigger [16], which is defined by a coincidence of 2 pads from the CIP and 2 pads from the COP, such that a straight line through all 4 pads intercepts the beam-axis (z-axis) within $\pm$ 44 cm of the nominal interaction point at $z = 0$. This indicates the presence of at least one charged particle in the central detector with a $p_T > 150$ MeV/c in the polar range 25° to 155°.

The central tracking system is complemented by a forward tracking system. All trackers are surrounded by a fine grained liquid argon sampling calorimeter [17], consisting of an electromagnetic section with lead absorbers and a hadronic section with steel absorbers.

3 Data Analysis

3.1 Event Selection and Background Reduction

The analysis is based on the 1992 sample of tagged events in which the energy of the scattered electron is measured in the H1 electron tagger. The event selection closely follows the one described in a previous letter on the determination of the absolute photoproduction cross section [18].

The fractional energy of the photon is called y, which in the case of the electron tagged events is well approximated by $y \approx 1 - (E_{e'}/E_e)$. Here E_e and $E_{e'}$ are the energy of the incoming and scattered electrons, respectively. The four-momentum transfer carried by the photon is denoted $Q^2 = 4E_eE_{e'}\cos^2(\theta/2)$. It depends on the electron energies and on the angle θ between the scattered electron and the proton beam direction.

The electron tagger acceptance is a function of y and Q^2. The cross section in the kinematic region seen by the electron tagger is calculated from the acceptance as a function of y, averaged over Q^2 up to the maximum Q^2 seen ($Q^2 < 10^{-2}$ GeV^2). To avoid ranges of small acceptance of the electron tagger, we restrict the analysis to the region $0.3 < y < 0.7$. These intervals in Q^2 and y define the kinematic region covered by the cross sections given below. As a consequence, the γp centre-of-mass energy range is 160 GeV $< \sqrt{s_{\gamma p}} = 2\sqrt{yE_eE_p} <$ 250 GeV, with an average of $\sqrt{s_{\gamma p}} \approx 200$ GeV.

Tagged events are required to have an electron candidate with energy $E_{e'} > 4$ GeV and to have less than $E_\gamma < 2$ GeV deposited in the photon detector. In addition, at least one ray trigger is required, ensuring activity in the central detector, and thus strongly suppressing electron beam induced background events.

After the track reconstruction only those events are retained, which have at least one track originating from the interaction region. In addition, we reject the following background events: beam-gas interaction events, characterized by more than 3 tracks originating in the downstream region (z < -100 cm, z at the point of closest approach to the z-axis); cosmic rays, identified as two collinear particle tracks; p-beam reactions in the beampipe itself, identified by the position of their $x - y$ vertex.

Interactions of the proton beam with the residual gas in the fiducial central region constitute the main remaining background. For tagged events, they appear in random coincidence with a signal in the electron tagger. The energy flow of such events is characterized by a value of $\sum p_z / \sum p$ close to 1, due to the large Lorentz-boost, and a small value of y_h. Here $y_h = \sum(E - p_z)/(2 \cdot E_e)$ is measured in the calorimeter where $\sum(E - p_z)$ is determined by summing $E \cdot (1 - \cos\theta)$ for all cells, and p_z denotes the longitudinal momentum component. As described previously in ref.[18], we reject the events in the region of small y_h and large $\sum p_z / \sum p$ *i.e.*, $y_h < 0.05$ *and* $\sum p_z / \sum p > 0.6$, or $y_h < 0.15$ *and* $\sum p_z / \sum p > 0.9$.

Due to the extended proton bunch length, the interaction region covers approximately ± 50 cm around the nominal interaction point. However, we accept only events with a z-position of the interaction vertex z_V (primary event vertex) within the central part of the detector, *i.e.*, $-25 < z_V < +25$ cm, restricting ourselves to a region of homogeneous track acceptance.

A total of 8467 events satisfy all described criteria. The remaining background is determined by analysing data from electron and proton pilot bunches. It is found to be less than 1% and is neglected.

3.2 Track Selection Criteria

The criteria below have been optimized to select particle tracks, originating from the primary vertex, for inclusion in the inclusive particle spectra:

- Transverse momentum $p_T > 0.3$ GeV/c.
- Pseudorapidity interval $|\eta| < 1.5$, with $\eta = -\ln \tan(\theta/2)$.
- $d/\sigma_d < 10$, where d is the distance of the extrapolated track from the primary vertex in the plane transverse to the beam axis, and σ_d the error of d.

- $| z_{TRACK} - z_V | < 10$ cm, with z_{TRACK} being the z-value of the track at the point of closest approach.
- Tracks must start radially within the first 3.5 cm of the tracker and be at least 15 cm long in the $x - y$ plane.
- The azimuthal angular range $160° < \phi(\text{track}) < 230°$ is excluded to avoid an inefficient region of the central drift chamber.

3.3 Corrections

In order to obtain the produced number of tracks, $N_{produced}$, the observed number of tracks is corrected with the following factors (errors given below denote statistical and systematic errors separately):

- A_{etag} : The geometrical acceptance of the electron tagger is corrected as a function of y and amounts to 55% in average for $0.3 < y < 0.7$. It is corrected per event. The tagger efficiency within the chosen acceptance is 100 % .
- ϵ_{trig} : The ray trigger efficiency depends on the number and topology of tracks. It is calculated independently for each event from the probability for each track to generate a ray. This probability is determined as a function of (p_T, θ) from data. The average value of ϵ_{trig} for all observed event topologies is $0.80 \pm 0.01 \pm 0.06$.
- ϵ_{event} : Two components in the event efficiency have to be considered:
  (i) The restriction of the primary event vertex to within $z = \pm 25$ cm is taken into account by a constant 67% efficiency factor, determined from the data. (ii) The efficiency for the event selection depends on the event topology. In particular, its value is 70 % for soft and 96 % for hard events (see below). Therefore, the efficiency as a function of p_T depends on the relative contribution of the two classes in a given p_T bin. Overall, the data sample is estimated to contain (75 ± 15)% soft and (25 ± 15)% hard events, based on the measured distribution of the maximum track p_T (see fig. 1 and discussion thereof). This introduces a small model dependence for the correction in the region $p_T < 1.5$ GeV/c, where both classes contribute.
  For the range $p_T > 1.5$ GeV/c where only hard events contribute, the total ϵ_{event} is found to be $0.64 \pm 0.02 \pm 0.02$.
- ϵ_{track} : The overall track efficiency is applied on a track by track basis. It contains three multiplicative components: (i) The efficiency for finding and reconstructing single tracks, ϵ_{reco}, is determined by visual scanning of tracks. It is found to be $(92 \pm 1 \pm 3)$% in the data and 100 % in the Monte Carlo simulation. (ii) The effect of the cuts applied in the track selection is determined by means of a Monte Carlo simulation (see below). The efficiency of these cuts, ϵ_{sel}, rises from 90 % at $p_T = 300$ MeV/c to 97 % at about 2 GeV/c , and remains constant beyond this value. The values are fitted with an empirical polynomial function in p_T (averaged over θ and ϕ) and then used to correct the p_T distributions. (iii) The ϕ-restriction of the geometrical acceptance of the central drift chamber (81%) is accounted for assuming a flat distribution in ϕ.
  The total ϵ_{track} is $0.73 \pm 0.05 \pm 0.05$ on average for $p_T > 1.5$ GeV/c.

An additional overall uncertainty of 7% from the luminosity measurement has to be added to the systematic errors. These 7% are not included in the error bars shown in the figures below. Tracks selected and corrected as discussed above have less than 3% contamination from non-primary tracks.

3.4 Monte Carlo Simulation Programs

Efficiencies and acceptance corrections of the cross sections partly rely on Monte Carlo simulations, which are based on the models described in the following.

Soft processes from low-p_T peripheral interactions are generated according to the vector dominance model with a Monte Carlo program based on the photoproduction event generator RAYPHOTON [19], using LUCVDM [20] for the soft meson-proton collision. Hard scattering events for direct and resolved γp interactions in leading order are generated with the PYTHIA 5.6 [21] program. The effects of initial and final state QCD radiation are described in PYTHIA by leading logarithm parton showers. For the structure functions we use GRV leading order parametrizations both for the proton [22] and the photon [9]. Note that the current knowledge of the photon structure function is based on measurements in two-photon interactions, which are primarily sensitive to the quark content only.

In both Monte Carlo programs the fragmentation of the partons into hadrons follows the Lund string model [23], as implemented in JETSET [21]. QED radiative corrections to the cross section are expected to be small $(2.5^{+1.4}_{-2.2})\%$ [18] for the present experimental conditions and are neglected.

The generated events are fed into the H1 detector simulation program, and then subjected to the same reconstruction and analysis chain as the real data. The detailed simulation of the detector parts is described in [13].

Processes involving a hard scattering are characterized by having a high value of p_T^{lead}, the p_T of the track with the largest p_T in the event. On the other hand, soft processes are not expected to exhibit large values of p_T^{lead}, since here the particle p_T essentially comes from hadronization. To illustrate that the Monte Carlo programs qualitatively describe the bulk of our data, we show in fig. 1 the observed uncorrected distribution of p_T^{lead} (full circles). The distribution is compared with predictions for the soft (dotted histogram) and hard (solid histogram) processes. Since a LO QCD calculation is divergent for $\hat{p}_T \to 0$, where $\hat{p}_T$ is the transverse momentum of the outgoing partons in the hard scattering process, a minimum p_T cut-off value $\hat{p}_T^{min}$ is applied in the PYTHIA generator. For this analyis this cut-off has been chosen to be $\hat{p}_T^{min} = 2.3$ GeV/c, in order to describe the observed spectrum as well as possible. The uncertainty in the composition of soft and hard contributions influences the efficiency calculation in the low p_T region and has been accounted for in the systematic errors (see above). Independent of the absolute rates, the soft component is limited to p_T-values below ≈ 1.5 GeV/c ; particles produced with p_T above 1.5 GeV/c originate predominately from interactions involving a hard collision.

4 Results on cross sections

The invariant cross section for single particle production is given by

$$\frac{\mathrm{d}^2\sigma}{\mathrm{d}p_T^2\ \mathrm{d}\eta_\circ} = \int \frac{\mathrm{d}^3\sigma}{\mathrm{d}p_T^2\ \mathrm{d}\eta_\circ \mathrm{d}\phi}\ \cdot \mathrm{d}\phi = \pi \cdot E \cdot \frac{\mathrm{d}^3\sigma}{\mathrm{d}p^3} \tag{1}$$

assuming azimuthal symmetry of the cross section and thus allowing the integration over ϕ. Here $\eta_\circ = -0.5 \cdot \ln((E-p_z)/(E+p_z))$ denotes the rapidity, which for $p >> m$ can be approximated by the pseudorapidity $\eta = -\ln(\tan(\theta/2))$, with p and m being the particle momentum and mass.

The cross section for inclusive charged particle production in ep collisions is calculated from the number of tracks produced, $N_{produced}$, in a bin of p_T and η by applying all efficiency and acceptance corrections to the observed track spectrum. It is given by :

$$\frac{\mathrm{d}^2\sigma}{\mathrm{d}p_T^2\ \mathrm{d}\eta} = \frac{N_{produced}(p_T,\eta)}{L \cdot 2p_T \Delta p_T \cdot \Delta\eta} \tag{2}$$

where L denotes the integrated luminosity. $\Delta\eta$ and $\Delta p_T^2 = 2 \cdot p_T \cdot \Delta p_T$ are the bin widths.

The resulting differential cross section for positively and negatively charged particles is shown in fig. 2. The error bars denote the quadratically combined systematic and statistical errors. The additional overall systematic uncertainty of 7 % from the luminosity measurement is not included in the figure. For the p_T spectra the η-range from -1.5 to 1.5 is used. The bin sizes in p_T are chosen such that bin migration is small, *i.e.,* less than 5%. The spectra are not unfolded for these small binning effects. The measured cross sections are listed in table 1. Note that the ep cross section is determined for the range $Q^2 < 10^{-2}$ GeV^2 and $0.3 < y < 0.7$. It can be converted into a γp cross section by taking into account the photon flux according to $\mathrm{d}\sigma = \sigma(\gamma p) \cdot Flux(y) \cdot \mathrm{d}y$. For the chosen y-range the integral over y of the photon flux yields a factor 74, assuming the Weizsäcker-Williams approximation [24].

In the same figure 2 are shown the cross section measurements by the UA1-collaboration [12] at the $\bar{p}p$ collider at $\sqrt{s} = 200$ GeV in the rapidity region $\eta <| 2.5 |$. In the γp CMS system the H1 data overlap with this rapidity interval in the photon hemisphere. The UA1 data points (open diamonds) are normalized to the H1 point at $p_T = 1.5$ GeV/c. The scale factor of order 4000 can be understood in terms of the the photon flux factor, the (ρ, ω, ϕ)-meson coupling constants within the VDM-model (of order 200), a factor π (see eqn. 1), a factor 1.5 (3 instead of 2 quarks in mesons versus baryons) and a factor 0.5 (UA1 numbers are for single charges only). In the range below 2 GeV/c , the p_T-spectra agree quite well. This shows that at low p_T photon-proton interactions are very similar to hadron-hadron interactions, as expected from the VDM picture.

However, more interesting is the difference observed in the p_T spectrum in the range above 2 GeV/c . The γp spectrum is clearly harder than the $\bar{p}p$ data. This can be seen quantitatively by fitting the following QCD inspired power-law [25] to the data:

$$E \cdot \frac{\mathrm{d}^3\sigma}{\mathrm{d}p^3} = A \cdot (1 + \frac{p_T}{(p_T)_0})^{-n}. \qquad (3)$$

Both spectra are well parametrized by eqn.(3). The UA1 data are described by the parameters [1, 12] $(p_T)_0 = (1.8 \pm 0.1)$ GeV/c and $n = 12.14 \pm 0.39$. A fit to our spectrum yields the values $(p_T)_0 = (0.63 \pm 0.20)$ GeV/c and $n = 7.1 \pm 2.0$. The fitted curves are indicated in fig. 2. The difference between the γp and *hadron* p scattering is further illustrated in fig. 2 by cross sections measured by the WA69 collaboration at CMS energies around 18 GeV [4]. Within the same experimental setup they determined the scattering cross sections with real photon and hadron $(= 60\%\pi + 40\% K)$ beams. Only the relative normalization of the two measurements (WA69-γ and WA69-h) is maintained. Two interesting observations result from these comparisons: a) at both small and large CMS energies, the γp data show a more pronounced tail at large transverse momenta compared to the *hadron* p data, b) both hadron-proton and γ-proton spectra harden with increasing CMS energy.

In fig. 3a we compare the measured p_T cross section above $p_T > 1.5$ GeV/c with the LO QCD calculation (PYTHIA). The full line represents the complete calculation including the resolved and direct processes. The calculation agrees well with the measured data in shape and in rate. The dashed line indicates the size of the resolved component, leaving a narrow band for the direct contribution between the dashed and full lines. As expected, the relative contribution of the direct process increases with transverse momentum of the particles [26]. Note that both the transverse momentum and the rapidity distributions of high p_T particles are related to the structure function of the photon: the cross section and form depends on the quark and gluon distributions in the photon as demonstrated, for instance, in ref.[26]. The dotted line in fig. 3a has been calculated using the resolved diagrams and the pion structure function [27] instead of the photon structure function in order to indicate the VDM piece of the full calculation. This latter calculation has been normalized at $p_T = 1.5$ GeV/c to the level of the total resolved

calculation, since the VDM component is expected to dominate at low transverse momenta. The difference between the dotted and the dashed lines therefore indicates the size of the anomalous part in the calculation. The latter is seen to make a significant contribution to the total.

The spectrum obtained using the pion structure function for the photon is still harder than the UA1 data which is expected for two reasons: firstly, parton momenta of quarks in mesons are on average larger than those of quarks in baryons. This simply provides more phase space for a high-p_T particle. Secondly, the variation of the CMS energy present for the photoproduction collisions leads to a small contribution towards a harder spectrum.

In fig. 3b the analytical NLO QCD calculation by B.A.Kniehl and G.Kramer [28] is compared with the measured data. The full line is the complete calculation which is in excellent agreement with the data, in shape as well as in absolute rate. The difference between the dashed and the full lines indicates again the contribution of the direct component.

The dependence of the cross section on the pseudorapidity η, $\mathrm{d}\sigma/\mathrm{d}\eta$, is shown in fig. 4 for all particles with $p_T > 1.5$ GeV/c . It has been corrected bin-by-bin for η-dependent effects. Binning effects are small and neglected. The high p_T-value was again chosen to suppress the soft processes. The measured cross sections are listed in table 2. The average number of produced charged particles with a p_T above 1.5 GeV/c is found to be $1.6 \pm 0.1 \pm 0.2$ per event, based on observations in a total of 749 events.

Note, that the η measured in the HERA frame is on average shifted by 2 units with respect to the η^* distribution in the γp CMS system. The spread of this shift due to the photon energy range is less than 0.3 units in pseudorapidity. Therefore the η and η^* distributions look very similar.

The full line in fig. 4 is the result of the NLO QCD calculation. Within the errors of the measurement the full calculation is compatible with the data. Again, the difference between the dashed and the full lines indicates the contribution of the direct photon processes. The LO calculation (PYTHIA) gives similar results.

Furthermore, a LO QCD calculation including parton showers using the HERWIG [29, 30] Monte Carlo program is found to agree with the measured cross sections in terms of the η- and p_T-variables.

5 Conclusions

We have measured the differential ep cross sections for charged particles in photoproduction events at HERA in the kinematic region $Q^2 \leq 0.01$ GeV^2 and $0.3 \leq y \leq 0.7$ for $\sqrt{s_{\gamma p}} \approx 200$ GeV.

Comparing the ep results with $\bar{p}p$ data at comparable CMS energies we find in the ep data an excess of particles in the region of large transverse momenta. According to QCD calculations, this is expected to be a reflection of direct and anomalous processes, which are predicted to be present in photoproduction, but absent in $\bar{p}p$ scattering.

The measured high p_T tail is also larger than has been observed in a previous photoproduction experiment. This effect results from the large increase of the CMS energy from $\sqrt{s_{\gamma p}} \approx 18$ GeV to $\sqrt{s_{\gamma p}} \approx 200$ GeV available at HERA.

The results from QCD calculations agree with the measured differential cross section in terms of the particle transverse momentum and pseudorapidity variables. The anomalous resolved process gives a sizeable contribution to the total cross section. This component, together with the direct processes, results in qualitatively different behaviour of photons and hadrons at high momentum transfers.

6 Acknowledgments

We are very grateful to the HERA machine group whose outstanding efforts made this experiment possible. We acknowledge the support of the DESY technical staff. We are grateful for the immense contributions of the engineers and technicians who constructed and now maintain the H1 detector. We thank the funding agencies for financial support. We also wish to thank the DESY directorate for the hospitality extended to the non-DESY members of the collaboration. We thank Bernd Kniehl for many helpful discussions.

References

[1] W.M.Geist *et al.,* Phys. Rep. 197 (1990) 263.

[2] H1 Collab., T. Ahmed *et al.,* Phys. Lett. B 297 (1992) 205.

[3] ZEUS Collab., M.Derrick *et al.,* Phys. Lett. B 297 (1992) 404.

[4] OMEGA Photon Collab., R.J.Apsimon *et al.,* Z. Phys. C 43 (1989) 63.

[5] ZEUS Collab., M.Derrick *et al.,* DESY 93-151 (1993).

[6] J.J.Sakurai, Ann. Phys. 11, (1960) 1;
M.Gell-Mann and F.Zachariasen, Phys. Rev. 124 (1961) 953.

[7] G.Wolf and P.Söding, in "Electromagnetic Interactions of Hadrons";
Vol.2, p.1; Eds. Donnachie and Shaw, 1978.

[8] Ch. Berger and W. Wagner, Phys. Rep. 146 (1987) 1;
H.Kolanoski and P.Zerwas, 'Two-Photon Physics' in 'High Energy
Electron-Positron Physics', eds. A.Ali and P.Söding, World Scientific 1988.

[9] M. Glück, E. Reya and A. Vogt, Phys. Rev. D 46 (1992) 1973.

[10] E.Witten, Nucl. Phys. B 120 (1977) 189.

[11] H1 Collab., I. Abt *et al.,* Phys. Lett. B 314 (1993) 436.

[12] UA1 Collab., Albajar, C. *et al.,* Nucl. Phys. B 335 (1990) 261.

[13] H1 Collab., I. Abt *et al., The H1 Detector at HERA*, DESY preprint 93-103 (1993).

[14] J.Bürger *et al.,* Nucl. Instr. Meth. A279 (1989) 217.

[15] K.Müller *et al.,* Nucl. Instr. Meth. A312 (1992) 457.

[16] S.Eichenberger *et al.,* Nucl. Instr. Meth. A323 (1992) 532.

[17] H1 calorimeter group, B.Andrieu *et al.,* Nucl. Instr. Meth. A336 (1993) 460.

[18] H1 Collab., T. Ahmed *et al.,* Phys. Lett. B 299 (1993) 374.

[19] N.H.Brook, A.DeRoeck and A.T.Doyle, RAYPHOTON 2.0,
Proc. HERA Workshop, DESY, Hamburg (1991), Vol. 3, p.1453.

[20] G.Ingelman and A.Weigend, Comp. Phys. Commun. 46 (1987) 241.

[21] T.Sjöstrand and M.Bengtsson, Comp. Phys. Commun. 43 (1987) 367;
H.-U.Bengtsson and T.Sjöstrand, Comp. Phys. Commun. 46 (1987) 43;
T.Sjöstrand, CERN-TH-6488 (1992).

[22] M. Glück, E. Reya and A. Vogt, Z. Phys. C 53 (1992) 127.

[23] Bo Andersson, G.Gustafson and T.Sjöstrand, Phys. Lett. B 94 (1980) 211;
Bo Andersson *et al.,* Phys. Rep. 97 (1983) 31.

[24] C.F.Weizsäcker, Z. Phys. 88 (1934) 612; E.J.Williams, Phys. Rev. 45 (1934) 729.

[25] R. Hagedorn, Riv. Nuovo Cim. 6 (1983) 1.

[26] F.M.Borzumati, B.A.Kniehl and G.Kramer, Z. Phys. C 59 (1993) 341.

[27] M. Glück, E. Reya and A. Vogt, Z. Phys. C 53 (1992) 651.

[28] B.A.Kniehl and G.Kramer, DESY 94-009 (1994).

[29] G. Marchesini *et al.,* Comp. Phys. Commun. 67 (1992) 465.

[30] G. Marchesini and B.R. Webber, Nucl. Phys. B 310 (1988) 461.

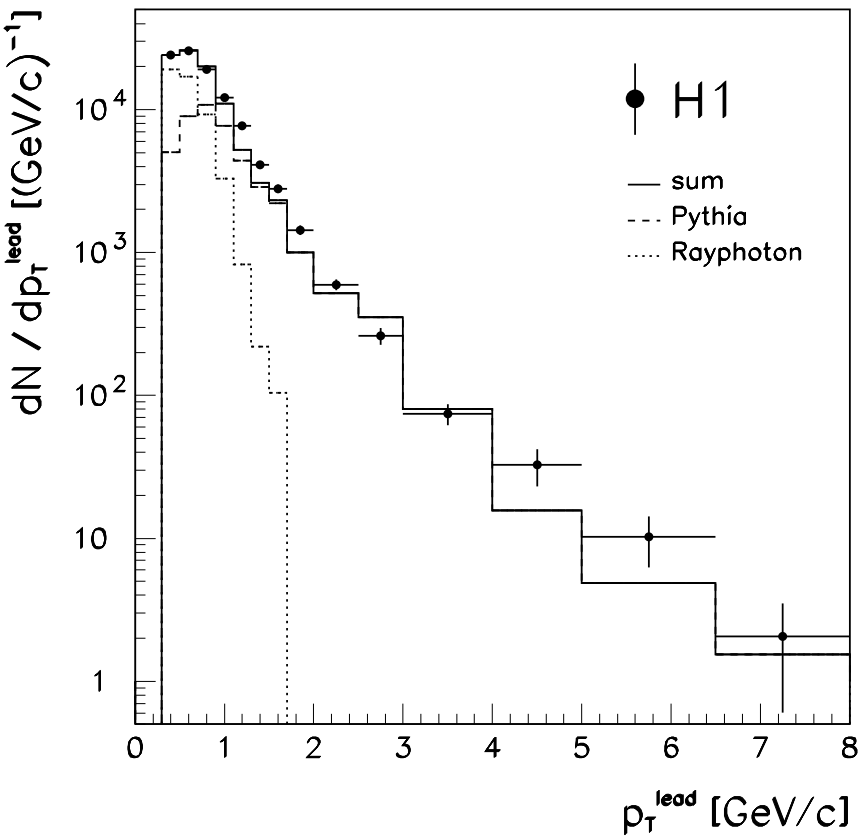

Figure 1: Measured uncorrected distribution of p_T^{lead}, the maximum track p_T in the event (full circles). The histograms represent the distributions for events simulated by the Monte Carlo programs PYTHIA(dashed) and RAYPHOTON(dotted) and their sum(full).

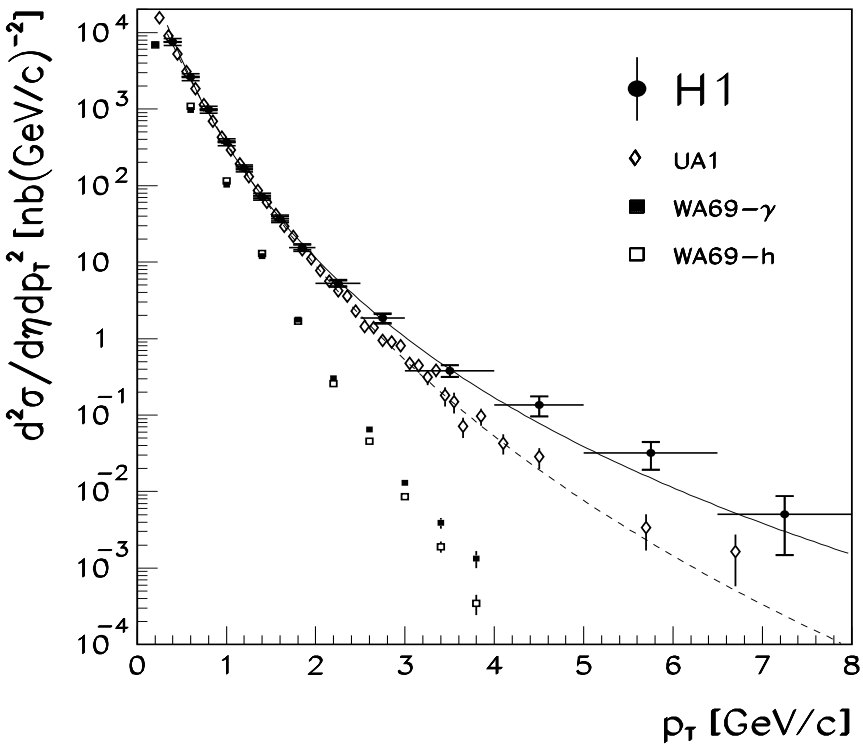

Figure 2: The inclusive ep cross section for charged particles in photoproduction (full circles) measured in the kinematical region $\mid \eta \mid < 1.5$, $Q^2 < 10^{-2}$ GeV^2 and $0.3 < y < 0.7$, at an average $E_{CMS}(\gamma p) \approx 200$ GeV. The error bars indicate the quadratic sum of statistical and systematic errors. An overall uncertainty of 7% from the luminosity measurement is not included in the figure. Also shown are cross sections measured by the UA1-collaboration (open diamonds) at $E_{CMS} \approx 200$ GeV for $\mid \eta \mid < 2.5$, normalized to the H1-data at $p_T = 1.5$ GeV/c. The curves indicate the power-law fit, as described in the text.
The rectangles show the shape of the cross section measurements by the WA69-collaboration at $E_{CMS} \approx 18$ GeV, for γp (filled rectangles) and for *hadron* p data (open rectangles).

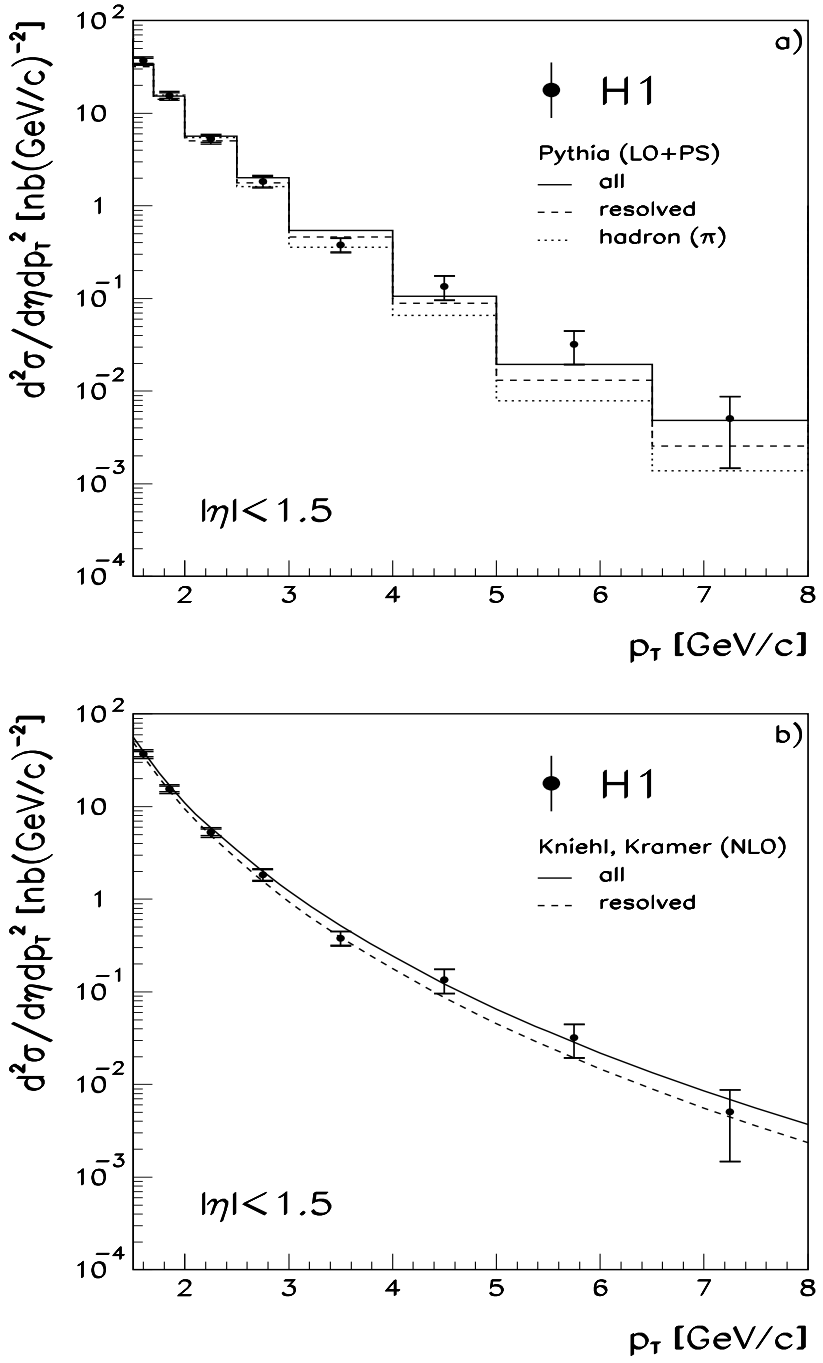

Figure 3: **a)** The measured cross section as depicted in fig. 2 (full circles) is compared in the $p_T > 1.5$ GeV/c region with the predictions of a LO QCD calculation (PYTHIA). The histograms indicate the different contributions to the calculation: resolved photon (dashed), all=resolved+direct (full), hadron using the pion structure function (dotted).
b) The same data points as in fig. 3a are compared with an analytical NLO QCD calculation [28]. The solid line represents the sum of the resolved (dashed line) and direct photon contributions.

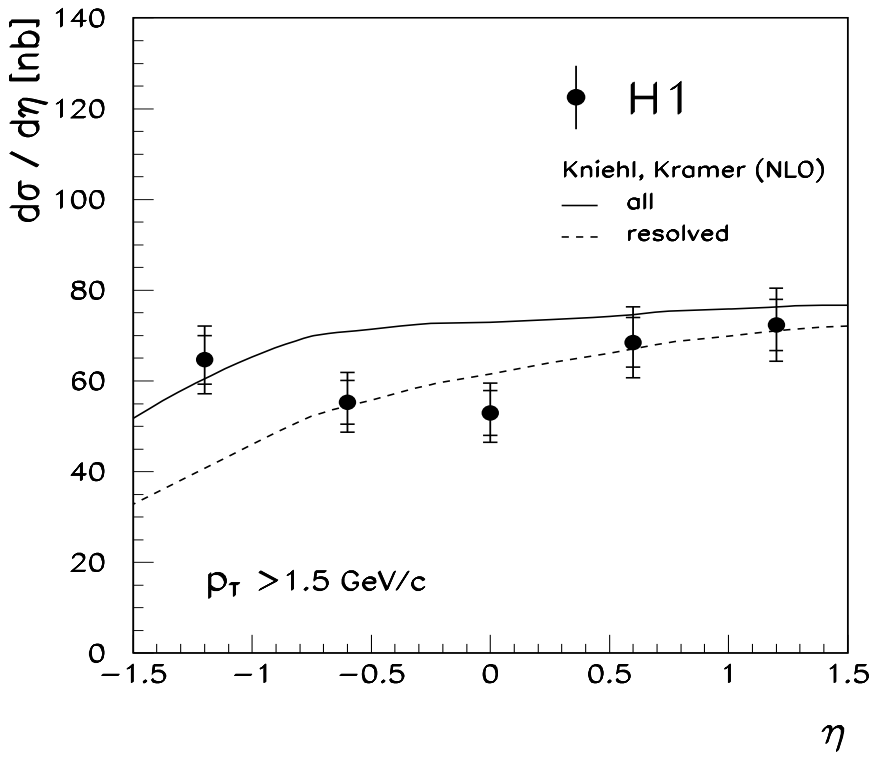

Figure 4: The measured differential ep cross section $\mathrm{d}\sigma/\mathrm{d}\eta$ for inclusive production of charged particles. Only particles with a $p_T > 1.5$ GeV/c are included. The outer (inner) error bars represent the total (statistical) errors. An overall uncertainty of 7% from the luminosity measurement is not included. The overlaid curves represent the prediction of the NLO QCD calculation [28]. The solid line represents the sum of the resolved (dashed line) and direct photon contributions.

Table 1: Measured differential cross section for the production of charged particles in the η-range -1.5 to 1.5. An overall uncertainty of 7% from the luminosity measurement is not included.

p_T [GeV/c]	$\frac{d^2\sigma^{ep}}{dp_T^2 d\eta}[\frac{\text{nb}}{(\text{GeV}/c)^2}]$	$\sigma_{stat}[\frac{\text{nb}}{(\text{GeV}/c)^2}]$	$\sigma_{syst}[\frac{\text{nb}}{(\text{GeV}/c)^2}]$
0.3−0.5	7547.5	78.7	734.0
0.5−0.7	2611.7	36.5	254.3
0.7−0.9	981.3	19.1	96.9
0.9−1.1	372.0	10.3	37.0
1.1−1.3	168.5	7.1	16.1
1.3−1.5	71.4	3.5	6.4
1.5−1.7	37.0	2.3	3.2
1.7−2.0	15.5	1.1	1.2
2.0−2.5	5.3	0.4	0.4
2.5−3.0	1.8	0.2	0.1
3.0−4.0	0.38	0.06	0.03
4.0−5.0	0.136	0.038	0.010
5.0−6.5	0.032	0.012	0.002
6.5−8.0	0.0050	0.0036	0.0004

Table 2: Measured differential cross section for the production of charged particles with $p_T > 1.5$ GeV/c. An overall uncertainty of 7% from the luminosity measurement is not included.

η			$\frac{d\sigma^{ep}}{d\eta}$[nb]	σ_{stat}[nb]	σ_{syst}[nb]
−1.5	–	−0.9	64.6	5.3	5.2
−0.9	–	−0.3	55.3	4.8	4.4
−0.3	–	0.3	53.0	5.0	4.2
0.3	–	0.9	68.5	5.5	5.5
0.9	–	1.5	72.4	5.6	5.8